BOULDER TRANSPORT BY HIGH-ENERGY (TSUNAMIS): MODEL DEVELOPMENT FOR THRESHOLD ENTRAINMENT AND TRANSPORT

N.A.K. NANDASENA [1] and Norio TANAKA [1]
[1] Hydraulic Engineering Lab., Department of Civil and Environmental Engineering, Saitama University

ABSTRACT

Coastal boulders are good evidence of high-energy events. Mathematical models are used to predict the magnitude of high-energy events from their boulders but the models are still in their preliminary stages. In a pioneering contribution, Nott (1997 and 2003) developed hydrodynamic equations to assess the minimum wave height required to initiate transport of a coastal boulder by tsunamis or storm surges. These equations are widely cited and used, but they can be improved. In this study, Nott's equations were revised. Boulder transport histogram was then introduced to predict the possible initial transport mode of a boulder from the flow velocity. These theoretical results were compared to field data, thus suggesting the initial transport mode of boulders and their pre-transport locations. Few studies have been conducted on modeling boulder transport by tsunamis despite the considerable research output on the analysis of boulder deposits. A detail description of derivation of governing equations for boulder transport in submerged, partially submerged, and subaerial (not in fluid contact) was presented and then a numerical model was proposed to solve the governing equations in one dimension. The model was validated by a well-controlled experimental study.

KEYWORDS: tsunami, boulder, numerical model, experiment

1. INTRODUCTION

Tsunami deposits have different characteristics in the nature. They could be either natural (sand, boulders) or artificial things. Tsunamis can bring large amount of sand and deposit them on the land as layers that basically exhibit the characteristics of landward and upward fining. The amount of sand to be deposited on the land is greatly controlled by the energy of the tsunami, topography and the availability/capacity of the source such size of a dune or beach/near-shore. Tsunamis can also transport big-boulders from near-shore or coast to land. This is not possible for all tsunamis because availability of boulder sources, pre-transport arrangement of boulders and the energy of the tsunami are the decisive factors to control boulder deposits on the land. In some cases, the back-wash (return flow) reworks the characteristics of the deposits.

Analysis on historic boulder deposits by paleo tsunamis or storms has long been a topic of interest in the field of geology/geomorphology and coastal hydraulics. The deposits could be presenting as an isolated boulder, scattered boulder fields or boulder clusters/ridges. The boulder deposits could be used to estimate the magnitude of historic tsunamis by inverse numerical modeling. However it has long been a challenging topic of interest because lack of good field observations, difficulty in identification of boulder sources, recognition of complex transport nature of boulders in turbulent fluid flows, and simplified assumptions for the theory developed. This study is conducted to develop numerical models to simulate the threshold entrainment and transport of boulders by tsunamis.

The prime aim of this study is to develop a numerical concept to find the magnitude (size) of historic tsunamis from their deposits (boulders). In order to reach the prime aim of this research study, following objectives are considered.

Review on previous works related to numerical modeling on boulder transport and inspect the possibility of improving their numerical concepts.

Develop governing equations to simulate threshold entrainment and transport of boulders by tsunamis and propose numerical solutions to the governing equations.

Conduct appropriate experimental studies to validate the numerical models.

2. MODEL DEVELOPMENT FOR THRESHOLD ENTRAINMENT OF BOULDERS BY TSUNAMIS/STORMS

Nott's equations have been revised: (1) the equation for the submerged boulder scenario has been revised by rearranging the lift area of the lift force, (2) the subaerial boulder scenario has been

reconsidered by rearranging lift area and omitting inappropriate use of inertia force, and (3) the joint bounded scenario was revised by balancing force components in the lifting direction, and the effect of slope at the pre-transport location is tested. Calculations are performed for four case studies: boulders in Western and Eastern Australia (data after Nott, 1997 and 2003), boulders in southeastern Italy (data after Scicchitano et al., 2007), storm boulders in Iceland (data after Etienne and Paris, 2010), and 2004 tsunami boulders in Sumatra (data after Paris et al., 2009).

2.1 Revised equations for initial transport of a boulder

The initial transport mode of a submerged or subaerial boulder will be sliding when:

$$u^2 \geq \frac{2(\rho_s/\rho_w - 1)gc(\mu\cos\theta + \sin\theta)}{C_d(c/b) + \mu_s C_l} \quad (1)$$

Initial transport of a submerged or subaerial boulder will be overturning/rolling when:

$$u^2 \geq \frac{2(\rho_s/\rho_w - 1)gc(\cos\theta + (c/b)\sin\theta)}{C_d(c^2/b^2) + C_l} \quad (2)$$

Initial transport of a submerged or subaerial boulder will be saltation when:

$$u^2 \geq \frac{2(\rho_s/\rho_w - 1)gc\cos\theta}{C_l} \quad (3)$$

Therefore, the initial transport of a submerged or subaerial boulder happens when:

$$u^2 \geq \min\left\{\begin{array}{l} \dfrac{2(\rho_s/\rho_w - 1)gc(\mu\cos\theta + \sin\theta)}{C_d(c/b) + \mu_s C_l} \\ \dfrac{2(\rho_s/\rho_w - 1)gc(\cos\theta + (c/b)\sin\theta)}{C_d(c^2/b^2) + C_l} \\ \dfrac{2(\rho_s/\rho_w - 1)gc\cos\theta}{C_l} \end{array}\right\} \quad (4)$$

where u is the flow velocity, ρ_b is the density of boulder, ρ_w is the density of fluid (1024 kg/m^3), g is the gravitational acceleration (9.81 m/s^2), μ_s is the coefficient of static friction between the boulder and the bed, θ is the ground slope at the pre-transport location, C_d is the coefficient of drag, b is the length of intermediate axis of boulder, c is the length of short axis (height), and C_l is the coefficient of lift.

If Eq. (4) is not satisfied, the boulder is stable against the fluid flow.

For the joint bounded boulder

$$u^2 \geq \frac{2(\rho_s/\rho_w - 1)gc(\cos\theta + \mu_s\sin\theta)}{C_l} \quad (5)$$

If Eq. (5) is not satisfied, the boulder is stable.

Different values of drag coefficient have been used in past studies, for example, 1.2 (Nott, 1997), 2.0–1.5 (Nott, 2003), and 1.95 (Noormets et al., 2004; Paris et al., 2010). Constants of 0.178 and 2.0, respectively, were taken as coefficients of lift and inertia (Nott, 1997 and 2003; Noormets et al., 2004 and Paris et al., 2010), and 0.7 as the coefficient of static friction (Noormets et al., 2004; Paris et al., 2010). In this study, 1.95, 0.178, 2.0 and 0.7 were chosen as coefficients of drag, lift, inertia, and static friction, respectively.

The difference between minimum flow velocities estimated by Nott's equations and our revised equations range between -65 and +214%. For the submerged scenario, velocities are reduced up to 56% (mean difference: -8%). Revision of the lift force equation explains the contrasting results for joint bounded blocks (-65 to +42%), for which lift force is essential, and subaerial boulders (-31 to +214%, mean difference +19%). Fig. 1 displays the correlation between the results from the revised and Nott's equations for all boulders considered in this paper. The effect of slope at the pre-transport location (in situ boulder) is not significant, because slope values of Lhok Nga are less than 2°. The results are changed only by 0.1 m/s compared to a horizontal bed. If we calculate the minimum flow velocity for calcareous boulders for slope angles 10°, 20°, and 30°, the mean flow velocity is increased by 0.3, 0.4, and 0.5 m/s, respectively compared to the horizontal bed, and for conglomerate megaclasts, increased by 0.6, 0.9, and 1.1 m/s.

Application of the boulder transport histogram to boulder accumulations in Iceland displays four distinct regions characterized by different properties (Fig. 2). The first region (white) represents the range of flow velocities that are not sufficient to initiate boulder transport (i.e., Eq. 4 or 5 is not satisfied). The second, third, and fourth regions represent the ranges of flow velocity to initiate the transport by sliding, rolling, and saltation, respectively. The fourth region has an open boundary at the top, but it is arbitrarily limited to 25 m/s. Most of the boulders in Iceland are not transported when the flow velocity is less than 4 m/s. For velocities higher than 6 m/s, most of the boulders are initially transported by rolling and saltation. Field observations of characteristics such as spatial distribution of fresh scars, striae, percussive marks, or crushing were used by

Etienne and Paris (2010) to confirm that storm boulders were moved by sliding, rolling, or saltation.

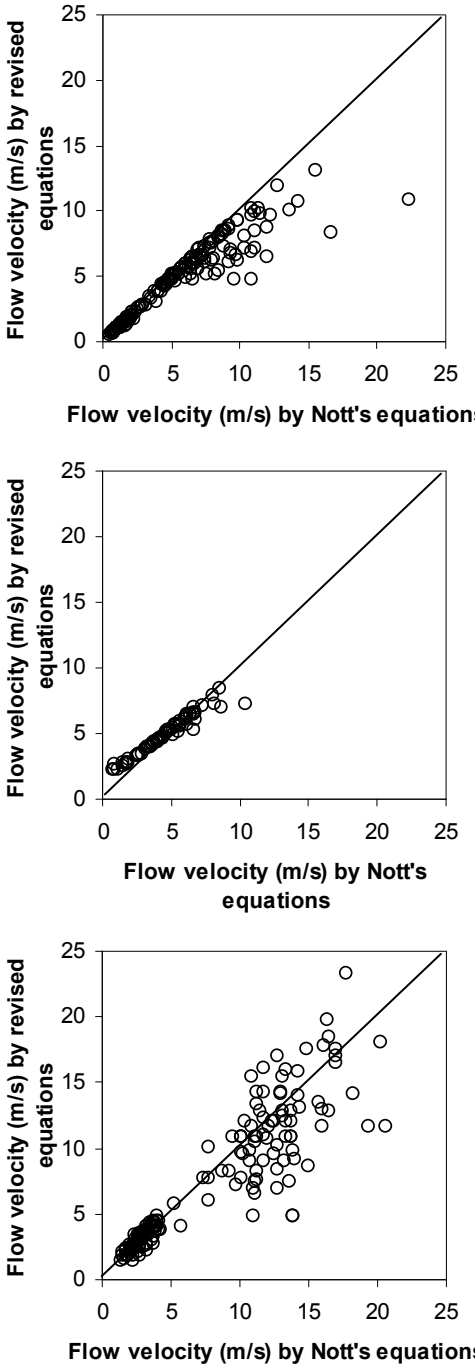

Fig. 1 – Plots of flow velocities according to Nott's equations and revised equations.

Figs. 3 to 6. display boulder transport histograms for boulders emplaced by the 2004 tsunami in Sumatra (Lhok Nga Bay). A tsunami generally strikes the coastal zone as a supercritical flow, the usual flow velocity of tsunami being estimated as 10–18 m/s (Nanayama and Shigeno, 2006 and references therein), and was estimated between 3 and 13 m/s at the nearshore during the 2004 tsunami in Lhok Nga Bay, Sumatra (Paris et al., 2010). This range of flow velocity is shown in histograms as a reference. Beach rock boulders, which are no larger than 2 m, are initially transported both by rolling and saltation (Fig. 3).

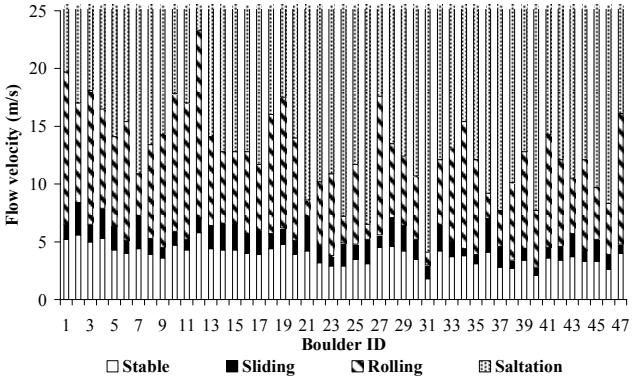

Fig. 2 – Boulder transport histogram for storm boulders in the Reykjanes Peninsula, Iceland (data after Etienne and Paris(2010)).

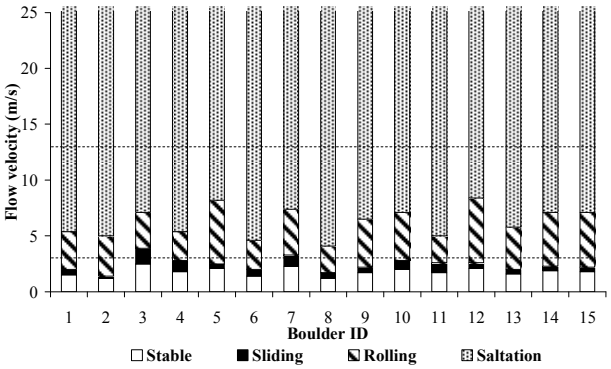

Fig. 3 – Boulder transport histogram for beach rock boulders in Sumatra (data after Paris et al.(2009)). Dotted lines show boundaries of flow velocity of the tsunami (3–13 m/s) on the coastal zone (estimated by Paris et al.(2010)).

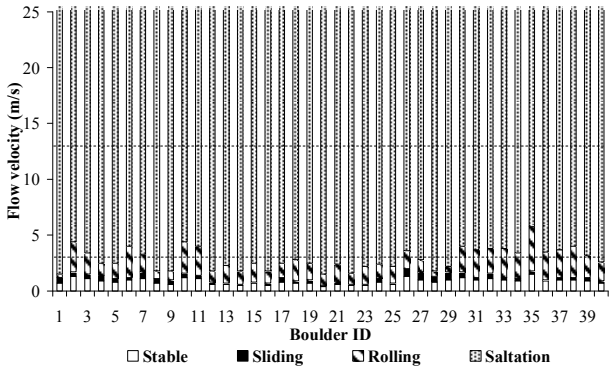

Fig. 4 – Boulder transport histogram for coral boulders in Sumatra (data after Paris et al.(2009)). Dotted lines show the boundaries of flow velocity of the tsunami (3–13 m/s) on the coastal zone (estimated by Paris et al.(2010)).

All coral boulders (Fig. 4 showing half of them) can also easily be moved by the tsunami flow, the dominant initial transport mode being saltation. Calcareous boulders from the seawall have higher densities (2.4 g/cm^3) than corals (~1.2 g/cm^3), and thus the required flow velocities are higher than 3–4 m/s to be transported by sliding or rolling, and higher than 11–12 m/s for saltation (Fig. 5). This is in good agreement with field observations by Paris et al. (2009), who noted that boulders from the seawall were deposited near their source (transport distance <280 m).

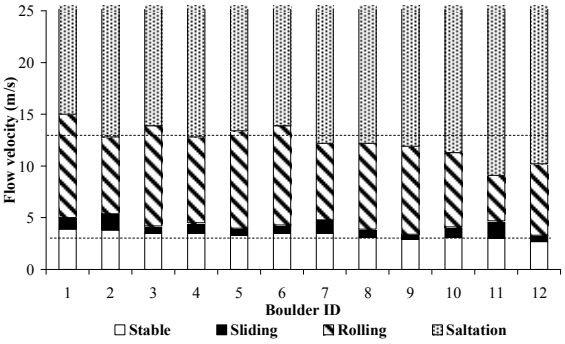

Fig. 5 – Boulder transport histogram for calcareous boulders from a seawall in Sumatra (data after Paris et al.(2009)). Dotted lines show the boundaries of flow velocity of the tsunami (3–13 m/s) on the coastal zone (estimated by Paris et al. (2010)).

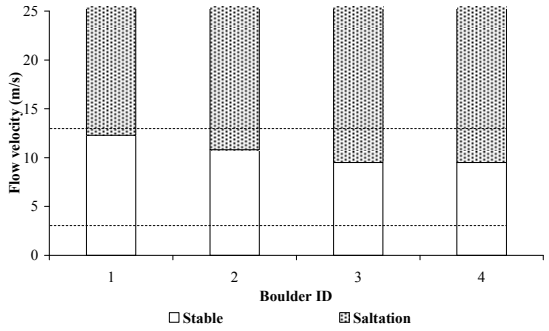

Fig. 6 – Boulder transport histogram for conglomerate boulders in Sumatra (data after Paris et al.(2009)). Dotted lines show the boundaries of flow velocity of the tsunami (3–13 m/s) on the coastal zone (estimated by Paris et al.(2010)).

Conglomerate boulders have only two regions in the histogram (Fig. 6), as these boulders were joint bounded in the pre-transport setting and lifted from their initial position. As shown in Fig. 6, flow velocities higher than 9–10 m/s are required to initiate their transport, whereas flow velocities estimated by Paris et al. (2010) are slower than 13 m/s. Thus, the model predictions are in good accordance with the distance transport observed for these plurimetric megaclasts.

3. MODEL DEVELOPMENT FOR BOULDER TRANSPORT BY TSUNAMIS

Boulder transport by fluid impact is complex and the three dimensional phenomena is simplified as follows. A boulder is regarded as a rectangular prism and the motion is restricted to sliding and saltation on a bed. The bed is impermeable and not eroding. Forces acting on the boulder are limited to the drag, lift, inertia, friction and reduced gravity force (vector summation of self weight and buoyancy). The tsunami force is perpendicular to the boulder face derived from the long and short axes (Fig. 7).

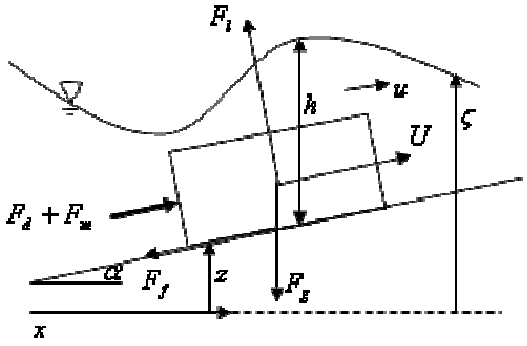

Fig. 7 – Detailed sketch of a boulder transported on a slope by a tsunami and its associated forces.

Where F_d = drag force, F_m = inertia force, F_f = friction force, F_l = lift force, u = current velocity near boulder, U = boulder velocity, h = water depth near boulder, F_g = reduced gravity force, α = slope of bed, ζ = water surface elevation measured from a datum, and z = bed elevation measured from the datum.

The momentum equation can be derived in such a way that the net force acting on the boulder is equal to the momentum changes of the boulder per unit of time as follows.

Boulder in submerged condition;

$$\begin{aligned}&\left(\rho_b^* + C_a\right) vol_b \left(dU/dt\right) - \left(1 + C_a\right) vol_b \left(Du/Dt\right) \\ &- \left(C_d A_D/2\right)\left|u - U\right|(u - U) + vol_b(\rho_b^* - 1) g\left(\partial z/\partial x\right) \\ &+ C_f \left\{ vol_b(\rho_b^* - 1) g\sqrt{1 - \left(\partial z/\partial x\right)^2} - \left(C_l A_l/2\right)(u - U)^2 \right\} \\ &\left(U/|U|\right) = 0 \end{aligned} \quad (6)$$

where $\rho_b^* = \rho_b / \rho$.

When a Boulder is transported in the partially submerged condition, the flow pattern around the boulder is rather chaotic compared to that in the

submerged condition. The impact of the boulder to water is also significant, thus the water depth around the boulder is varied significantly and the flow exhibits characteristics of turbulence. However, simplifying the complexity associated with, Eq. (6) can be revised for partially submerged condition by imposing the ratio of water depth to boulder height as follows. The lift force is omitted.

$$\begin{aligned}&\left\{\rho_b^* + C_a\left(h/h_b\right)\right\}vol_b\left(dU/dt\right)\\&-(1+C_m)\left(h/h_b\right)vol_b\left(Du/Dt\right)-\left(C_d A_d h/2h_b\right)\left|u-U\right|(u-U)\\&-vol_b\left(\rho_b^* - h/h_b\right)g\left(\partial z/\partial x\right)\\&+C_f vol_b\left(\rho_b^* - h/h_b\right)g\sqrt{1-\left(\partial z/\partial x\right)^2}\left(U/\left|U\right|\right)=0\end{aligned} \quad (7)$$

The boulder is subjected to the friction force and self weight when it transports in subaerial condition. The momentum equation can be derived as follows.

$$dU/dt + g\left(\partial z/\partial x\right) + C_f g\sqrt{1-\left(\partial z/\partial x\right)^2}\left(U/\left|U\right|\right)=0 \quad (8)$$

Depth integrated shallow water equations are used to simulate tsunami propagation in ocean and run up on ground. The equations are written as follows.

$$\partial\varsigma/\partial t + \partial Q/\partial x = 0 \quad (9)$$

$$\partial Q/\partial t + \frac{\partial\left(Q^2/h\right)}{\partial x} + gh\left(\partial\varsigma/\partial x\right) + \tau/\rho = 0 \quad (10)$$

where Q = discharge per unit width (= uh), τ = bed roughness on water, $\tau = \rho g n_m^2 Q^2/h^{7/3}$ where n_m = Manning's roughness coefficient.

Therefore Eqs (6 to 10) govern the transport of a boulder by tsunami induced force (long period wave).

3.1 Limitations of the model

1. A boulder is considered to be a homogeneous cubic/or rectangular prism. The initial orientation of a boulder considers that the long axis of the boulder is perpendicular to the tsunami direction; thus, the model assumes constant drag and lift areas during the transport.

A boulder in the field is neither cubic nor rectangular and heterogeneous; thus the numerical model usually underestimates or overestimates its weight. As the boulder is subjected to complex motion, fixed projected areas for force calculation are not always conservative. Lorang (2000) simulated different boulder movements and found that transportability was strongly influenced by the boulder shape.

2. The pre-transport environment of a boulder is important (Pignatelli et al., 2009; Goto et al., 2010), but the model simplifies the boulder to be isolated (single), detached, and not buttressed.

3. Previous models of boulder transport assumed sliding as a mode of transport for a boulder (Noji et al., 1993; Imamura et al., 2001), but boulders in the experiments of Imamura et al. (2008) are mainly seen to be transported by a bore due to rolling or saltation rather than by sliding. Experimental studies showed that the transport mode can vary depending on the current velocity, bottom friction, and shape and weight of the boulder (Goto and Imamura, 2007). Our new model takes sliding and saltation into account. Rolling is a very complex phenomenon. One approach is to consider rolling in the model by reducing dynamic friction. This is not theoretical, but uses extensive experimental studies to develop an empirical relationship (e.g., Imamura et al. (2008) found such a relationship by doing limited experimental studies). The other approach is to consider the concept of angular momentum. This is theoretical. In this case, the hydraulic moment is more appropriate than hydraulic force applied to a boulder to calculate the boulder velocity and transport distance.

4. Constant force coefficients are used in the numerical simulation, and they are obtained from past studies. As in Noji et al. (1993), these coefficients are time dependant and functions of the Froude number and relative water depth. Therefore, a precise estimation of these coefficients at the site concerned should be attempted.

5. Boulder-to-boulder interactions (collisions and shielding effects) are disregarded. These interactions during boulder transport, as evidenced by striae, percussive marks, or crushing on the surface of the boulders, were observed by Paris et al. (2009) during a field survey in January 2005.

6. The depth-averaged flow structure around the boulder is considered and the model disregards the micro-topographical changes, but these parameters could be important in boulder transport.

4. EXPERIMENTAL STUDY

An experimental study was conducted to validate the numerical model in a flume (18 m long, 0.4 m wide, and 0.75 m height) in the hydraulic engineering laboratory, Saitama University. The flume bed was made of plain wood and that has a 1:20 slope continuing from a flat bed (Fig. 8). Tsunami overland flow was generated by rapidly opening a hinged gate, so called "dam-break" of a water tank on the flat bed. Four water depths in the tank were selected: H = 30, 25, 20, and 15 cm (hereinafter dam-break height) that have potential to make the turbulent flows of strong to weak on the slope. A set of wave gauges, G0-G11

(ultrasonic type; UD-500 KEYENCE, accuracy 0.1 mm) and current meters (propeller type; VO2103 KENEK, measuring range 3-200 cm/s, accuracy 3 cm/s) was deployed with each spacing 0.5 m to measure flow depth and flow velocity on the slope. The data were measured at frequency of 10 Hz. The models of boulders were made of natural limestone and coral. In addition, the boulder models of cement were made to represent lighter boulders such as porous coral boulders. The average wet densities of the models of limestone, coral, and cement were 2.76, 2.18, and 1.8 g/cm^3 respectively. Fifteen boulder models of axes-dimensions varying from 1.5 to 8 cm with the shapes of cubic and rectangular and the flatness index (Cailleux and Tricart, 1959) ranging from 1.0 to 3.0 were tested (Table 1). Four video cameras, VC1-4 (Olympus) were placed to record the transport of blocks on the slope. Straight lines, each at 10 cm spacing, were drawn on the slope bed to calculate the velocity of blocks during the transport.

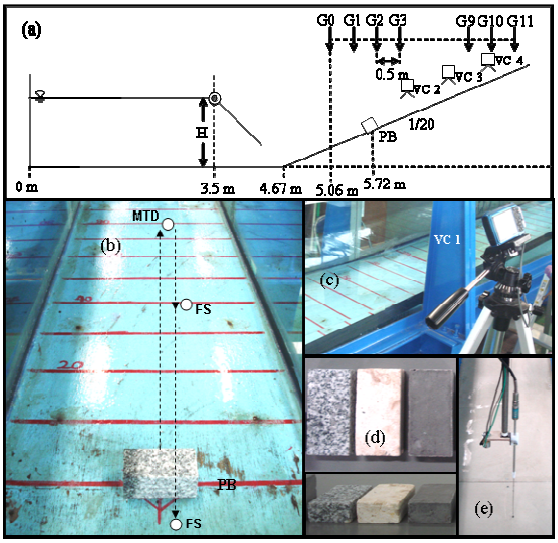

Fig. 8 – Experimental setup, (a) schematic sketch of experimental setup, G0-11 are locations of wave gauge and current meter, VC1- 4 are video cameras, PB is the pre-transport location of a block, H is the initial water depth in the tank (dam-break height), (b) slope bed and the block prior to transport, MTD is the maximum transport distance (first stop), FS is the final stop (c) A video camera (VC1) focusing the pre-transport location of the block, (d) models of boulders: blocks of limestone, coral, and cement (synthetic), (e) Ultrasonic type wave gauge and propeller type current meter.

Table 1 – Characteristics of boulder models. Note that a, b, and c are the lengths of long, intermediate, and short (height) axes of the blocks respectively.

Block type	Dimension (cm) (a x b x c)	Flatness Index $(a+b)/2c$	Wet density kg/m^3
Limestone (Li)	8 x 4 x 4	1.5	2629 – 2880 average (2760)
	6 x 4 x 4	1.25	
	4 x 4 x 4	1	
	8 x 4 x 2	3	
	6 x 4 x 2	2.5	
	2 x 2 x 2	1	
Coral (Co)	8 x 4 x 2	3	2333 – 2054 average (2180)
	6 x 4 x 2	2.5	
	2 x 2 x 2	1	
Synthetic (Ce)	8 x 4 x 4	1.5	1985-1723 average (1800)
	6 x 4 x 4	1.25	
	4 x 4 x 4	1	
	8 x 4 x 2	3	
	6 x 4 x 2	2.5	
	1.5 x 1.5 x 1.5	1	

First, the experiments without the blocks were conducted and the characteristics of the flow (flow depth and flow velocity) were measured. Second, the experiments with the blocks were conducted. Each block was placed with the long axis perpendicular to the flow direction at the pre-transport location (PB-Fig. 8) prior to the fluid flow hit the block. In addition, different pre-transport orientations of the long axis of the block to the flow and the effect of number of the blocks (interaction) on the transport distance were tested. Each test was conducted at least three times (test trials) for the accuracy of the results and out of the three tests, one test was videoed. The spatial progress of the blocks and the velocity were estimated by analyzing frames which were extracted at 0.1 s intervals from the video footages.

The blocks with the flatness numbers between two to three were transported mainly due to sliding and a few smaller blocks with the flatness number one were moved mainly due to rolling. Rolling was not always about the main axis as it was set in the beginning, but was about different axes with time. In some cases, the blocks were transported due to both sliding and rolling despite the flatness number of the block. For such cases, rolling was initiated primarily due to the effect of macro-roughness of the slope bed (e.g. construction joints of wooden planks of the slope bed). The blocks were hardly any transported due to saltation. The blocks had two stops during its transport: the first, after reaching the maximum transport distance by the run-up flow; the block stopped temporarily during the flow transition and the second, the permanent stop after the run-down flow for a single dam-break flow. Most of the blocks were transported up-slope by the run-up flow and returned (or passed) the pre-transport location by the run-down flow whereas a few blocks stopped before reaching the pre-transport location. We have observed secondary motions during sliding of the blocks: swing (i.e. back and forth motion of edges of the block) and rotation on the slope bed. This may be due to both the change in friction between the block and the bed and change in hydraulic force applied on the block or either. Such secondary motions were not observed/or a very few during the transport by the run-down flow.

4.1 Model validation

Except the coefficient of friction, the other coefficients: drag (1.95), lift (0.178), and added mass (1.0) are referred from the previous studies (Nott, 2003; Paris et al., 2010). It was reported that

the coefficient of drag is sensitive to Froude number (Noji et al., 1993) and the orientation of the body to the fluid flow (Hoerner, 1965). We however use a constant coefficient for the drag (1.95) as an initial step of the study. The coefficient of friction was estimated by dragging with relatively small velocity the blocks along the slope bed under the wet condition and measuring the force for motion by a digital force gauge (RX-10 AIKOH, measuring range 0-100 N, accuracy 0.2 N). Fig. 9 displays the temporal variation of friction coefficient between the block and slope bed.

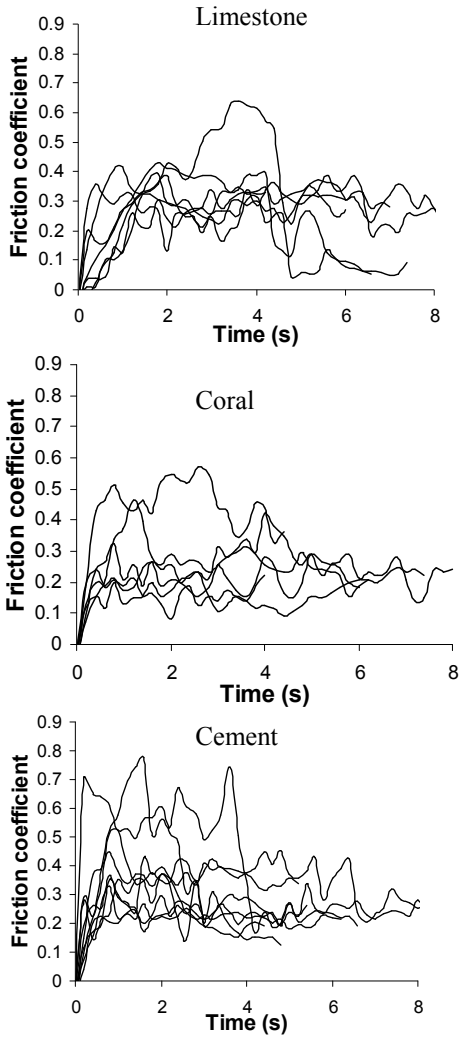

Fig. 9 – Time history of friction coefficient for the blocks in motion.

It seems the coefficient can not be taken as a constant as the variance in magnitude is significant. The greater variations in the coefficient of friction are attributed to the change in roughness due to the spatial change of the texture of the wood of the slope bed. Therefore, the upper and lower limits of the coefficient were defined rather than taking an averaged value, which satisfy all the blocks tested. The upper limits for the coefficients of static and dynamic fictions are 0.7 and 0.5, and the lower limits are 0.4 and 0.2 respectively (Fig. 9). The numerical modeling was done twice for each test with the upper and lower limits of the coefficient of friction.

Even though we maintained the accuracy of dam-break flow, the maximum transport distance on the slop-bed was different for the each test of the block for the same dam-break flow. The transport path of the block for the each test was different, which was influenced greatly by the friction of the slope-bed (Fig. 9) and modes of secondary transport such as swing-motion and rotations on the slope bed. Therefore we hardly any observed the same maximum transport distance for a single block during its three trials. Fig. 10 displays the comparison between the numerical and experimental results for a limestone block transported by the dam-break height of 30 cm.

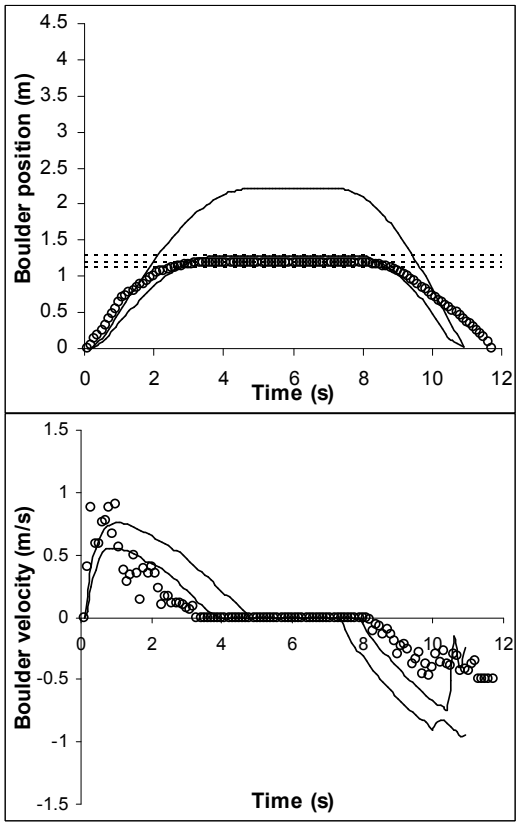

Fig. 10 - Comparison between the modeling and experimental results for Li – (6 x 4 x 4) – H = 30. Note that dashed line shows maximum transport distance of the block for test trials, circles indicate experimental results, and continuous line displays numerical results for the upper and lower limits of the friction.

The trend of modeling results well agrees with the pattern of experimental results despite the exact overlapping each other. For all most all the test cases, the rage of maximum transport distance

predicted by the model agrees with the observed range in the experiments. Fig. 11, Li-(4 x 4 x 4) – H = 30 shows a significant mismatch between the transport times of the block: the model predicted time is higher than the measured time in the experiment. This is due to the rotation of the block on the slope bed during the transport, thus the main transport mode sliding was hindered. Such a complex motion can not be simulated by the model.

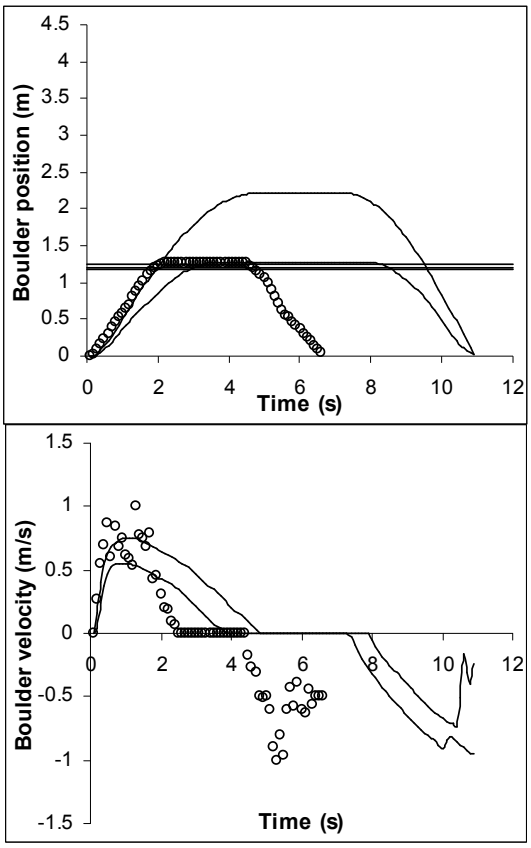

Fig. 11 - Comparison between the modeling and experimental results for Li – (6 x 4 x 4) – H = 30.

The numerical model underestimates the velocity of the block in the beginning of the transport compared to that of measured in the experiments. We observed that the wave front hit the block with vertical spraying (splashing) and then covered the block with water in a very small time (0.1-0.4 s). There could be an impact force associated with the vertical spraying, that could increase in the velocity of the block in the beginning. The model predicts the velocity of the block reasonably well during the backward transport. We did not observe any complex flow patterns like vertical spraying during the backward transport of the block.

The small blocks (Li – 2 x 2 x 2, Co – 2 x 2 x 2, and Ce – 1.5 x 1.5 x 1.5, Table 1) were transported due to rolling by the dam-break flow of 30 cm. The model also predicts the same transport mode for the blocks with the upper limits of the friction during the forward motion. Axis of rolling of the block observed in the experiment was different whereas the model assumes uni-axial rolling. For the platy blocks of cement (Ce – (8 x 4 x 2 and 6 x 4 x 2) – H = 30), the model with the high friction predicts rolling during upslope transport whereas both sliding and rolling were observed in the experiment. The model predicts the experimental results of block transport more accurately for the dam-break heights of 25, 20, and 15 cm compared to that of the dam-break of 30 cm. The predicted initial velocity of the block well agrees with the measurement in the experiments. We did not observe significant vertical spraying when the wave front hit the block, thus the effect of impact force could not to be significant. In addition, secondary transport modes like rotation and swing were not observed during the experiment. The conditions of the experiment well conjugated the theory developed in the model, thus reproducing the experimental results with a good accuracy. The smallest block (Fig. 12) was only transported by the dam-break height of 15 cm. It stopped after reaching the maximum transport distance and the model also predicted the same.

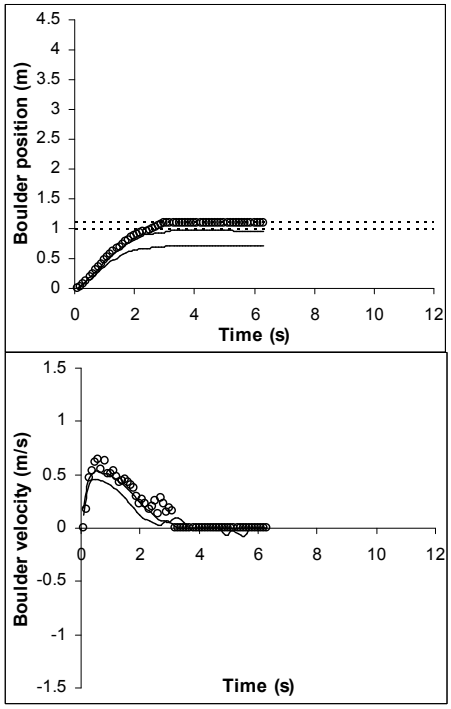

Fig. 12 - Comparison between the modeling and experimental results for Ce – (1.5 x 1.5 x 1.5) – H = 15.

5. CONCLUSIONS

The hydrodynamic equations derived by Nott (1997 and 2003) are a simple and useful tool for predicting the initial transport of a boulder by tsunamis or storm surges, but they can be improved. In this study, Nott's equations were revised: (1) the equation for submerged boulder scenario was

revised by rearranging the lift area of the lift force, (2) the subaerial boulder scenario was reconsidered by rearranging the lift area and omitting inappropriate use of inertia force, and (3) the joint bounded scenario was revised by balancing force components in the lifting direction, and the effect of the slope at pre-transport location was tested.

The differences between the results obtained from Nott's equations and the revised equations were discussed for four cases (representing a population of 244 boulders). The minimum flow velocity required to initiate the transport of submerged boulders from the revised equation is less than that from Nott's equation (e.g. reduced up to 56% for submerged boulders, 65% for joint bounded blocks). This is attributed to the increment of the lift area in the revised equation. The minimum flow velocity required to initiate the transport of subaerial boulders from the revised equation also differed in comparison with the results of Nott's equation (e.g., 4–22% for boulders detached from a seawall by the 2004 tsunami in Sumatra), while the latter is not applicable for some boulders (e.g., beach rock boulders transported from the near shore by the 2004 tsunami). This is attributed to an inappropriate use of inertia in Nott's equation. If we consider a joint bounded scenario for storm boulders in Iceland, the minimum flow velocity varies from -43 to +41% compared to that derived by Nott's equation. The negative and positive percentages correspond to the increment in the lift force against the self weight of the boulder and vice versa in the revised equation. The mean difference between the results of the revised equations and Nott's equations range between -8 % (submerged) and +19% (subaerial) for the 244 boulders analyzed.

A graphic tool called the 'boulder transport histogram' that represents the range of flow velocities required for the initial transport of a boulder in different modes: sliding, rolling, and saltation, was introduced. The boulder transport histogram can be used to predict the possible initial transport mode of a boulder with a given flow velocity. These theoretical results were compared to field data, and the initial transport mode of boulders from different ranges of flow velocities can be found. The numerical model fits particularly well with velocities estimated for the 2004 tsunami in Lhok Nga Bay (Sumatra). The boulder transport histogram could be a valuable tool to reconstruct the magnitude of prehistoric extreme energy events such as tsunamis or storm surges in terms of flow velocity.

Governing equations for boulder transport by tsunamis in submerged, partially submerged and subaerial (not in fluid contact) conditions were derived from Nott's original equations (1997, 2003). A new numerical solution to the governing equations along with equations for tsunami-induced flow was proposed.

Well controlled experimental studies are required to validate the numerical models of boulder transport by tsunamis prior to use for analyzing the observations of boulders in the field. Such experimental studies are extremely rare in the previous studies. An experimental study was conducted to validate the numerical model. The model can simulate the boulder transport due to sliding, rolling, and saltation. The underlying theories for modeling these transport modes are associated with numerous assumptions. Boulders were simply modeled by cubic/rectangular (flatness number varying from one to three) blocks with different densities. The simplified shape is one of great assumptions in order to reduce in complexity of calculation of applying forces/moments to the boulders. Tsunami overland flow was simulated by dam-break flow. The blocks with the flatness numbers between two to three were transported mainly due to sliding and a few smaller blocks with the flatness number one were moved mainly due to rolling. In some cases, the blocks were transported due to both sliding and rolling despite the flatness number of the block. The change of transport mode was mainly attributed to the friction (macro roughness) between the bed and the block. The blocks were hardly any transported due to saltation. The numerical model was able to reproduce the experimental observations fairly well. The difference between modeling and experimental results was mainly attributed to the secondary motions likely swing and rotation due to both the variable friction and fluid forces applied to the blocks.

6. REFERENCES

Barbano, M.S., Pirrotta, C., Gerardi, F., 2010. Large boulders along the south-eastern Ionian coast of Sicily: Storm or tsunami deposits? *Marine Geology*, Vol.275, pp.140-154.

Benner, R., Browne, T., Brückner, H., Kelletat, D., Scheffers, A., 2010. Boulder Transport by Waves: Progress in Physical Modelling. *Zeitsch. Geomorphologie*, Vol.54, pp.127-146.

Bourgeois, J., Mac Innes, B., 2010. Tsunami boulder transport and other dramatic effects of the 15 November 2006 central Kuril Islands tsunami on the island of Matua. *Zeitschrift für Geomorphologie*, Vol. 54, pp.175-195.

Cailleux, A., Tricart, J., 1959. Contribution a l'etude des sables et des galets. CDU, Paris. 376 pp.

Engel, M., May, S., M., in press. Bonaire's boulder fields revisited: evidence for Holocene tsunami impact on the Leeward Antilles. Quaternary Science Reviews.

Etienne, S., Paris, R., 2010. Boulder accumulations related to storms on the south coast

of the Reykjanes Peninsula (Iceland). *Geomorphology*, Vol.114, pp.55-70.

Etienne, S., Buckley, M., Paris, R., Nandasena, A.K., Clark, K., Strotz, L., Chagué-Goff, C., Goff, J., Richmond, B., 2011. The use of boulders for characterising past tsunamis: lessons from the 2004 Indian Ocean and 2009 South Pacific tsunamis. *Earth Science Reviews*, Vol.107, pp.79-90.

Fritz, H.M., Borrero, J.C., Synolakis, C.E., Yoo, J., 2006. 2004 Indian Ocean tsunami flow velocity measurements from survivor videos. *Geophysical Research Letters*, Vol.33, L24605.

Goff, J., Weiss, R., Courtney, C., Dominey-Howes, D., 2010. Testing the hypothesis for tsunami boulder deposition from suspension. *Marine Geology*, Vol.277, pp.73-77.

Goto, K., Imamura, F., 2007. Numerical models for sediment transport by tsunamis. *The Quaternary Research* (Daiyonki-Kenkyo) , Vol.46, pp.463-475.

Goto, K., Chavanich, S.A., Imamura, F., Kunthasap, P., Matsui, T., Minoura, K., Sugawara, D., Yanagisawa, H, 2007. Distribution, origin and transport process of boulders deposited by the 2004 Indian Ocean tsunami at Pakarang Cape, Thailand. *Sedimentary Geology*, Vol.202, pp.821-837.

Goto, K., Okada, K., Imamura, F., 2009a. Characteristics and hydrodynamics of boulders transported by storm waves at Kudaka Island, *Japan. Marine Geology*, Vol.262, pp.14-24.

Goto, K., Okada, K., Imamura, F., 2009b. Importance of the Initial Waveform and Coastal Profile for Tsunami Transport of Boulders. Polish *Journal of Environmental Studies*, Vol.18, pp.53-61.

Goto, K., Kawana, T., Imamura, F., 2010a. Historical and geological evidence of boulders deposited by tsunamis deposited by tsunamis, southern Ryukyu Islands, Japan. *Earth-Science Review*, Vol.102, pp.77-99.

Goto, K., Okada, K., Imamura, F., 2010b. Numerical analysis of boulder transport by the 2004 Indian Ocean tsunami at Pakarang Cape, Thailand. *Marine Geology*, Vol.268, pp.97-105.

Goto, K., Miyagi, K., Kawana, T., Takahashi, J., Imamura, F., 2011. Emplacement and movement of boulders by known storm waves — Field evidence from the Okinawa Islands, Japan. *Marine Geology*, Vol.283, pp.66-78.

Hall, A.M., Hansom, J.D., Williams, D.M., 2010. Wave-emplaced coarse debris and megaclasts in Ireland and Scotland: boulder transport in high-energy littoral environment: a discussion. *Journal of Geology*, Vol.118, pp.699-704.

Hansom, J.D., Barltrop N.D.P., Hall, A.M., 2008. Modelling the processes of clip-top erosion and deposition under extreme storm waves. *Marine Geology*, Vol.253, pp.36-50.

Harada, K. and Imamura, F., 2006. Effects of coastal forest on tsunami hazard mitigation— A preliminary investigation. Published in Tsunamis: Case Studies and Recent Development, ed. K. Satake (Advances in natural and Technological Hazards Research, Springer), pp. 279–292.

Hoerner, S.F., 1965. Fluid dynamic drag, pp. 3.1-3.28, published by the author.

Imamura, F., Yoshida, I., Moore, A., 2001. Numerical study of the 1771 Meiwa tsunami at Ishigaki Island, Okinawa and the movement of the tsunami stones. *Annual Journal of Coastal Engineering, JSCE*, Vol.48, pp.346–350.

Imamura, F., Goto, K., Ohkubo, S., 2008. A numerical model for the transport of a boulder by tsunami. *Journal of Geophysical Research*, Vol.113, C01008. doi: 10.1029/2007JC004170.

Kawata, Y., Benson, B., Borrero, J., Davies, H., do Lange, W., Imamura, F., Letz, H., Nott, J., Synolakis, C.E., 1999. Tsunami in Papua New Guinea not as intense as first thought. *Trans. Am. Geophys. U.* , Vol.80, EOS, pp.101-105.

Kennedy, D.M., Tannock, K.L., Crozier, M.J., Rieser, U., 2007. Boulder of MIS 5 age deposited by a tsunami on the coast of Otago, New Zealand. *Sedimentary Geology*, Vol.200, pp.222-231.

Kogure, T., Matsukura, Y., 2010. Instability of coral limestone cliffs due to extreme waves. *Earth Surf. Process. Landforms*, Vol.35, pp.1357-1367.

Lange, W.P.D, Lange, P.J.D., Moon, V.G., 2006. Boulder transport by waterspouts: An example from Aorangi Island, New Zealand. *Marine Geology*, Vol.230, pp.115-125.

Lavigne, F., Paris, R., Wassmer, P., Gomez, C., Brunstein, D., Grancher, D., Vautier, F., Sartohadi, J., Setiawan, A., Syahnan, Gunawan, T., Fachrizal, Waluyo, B., Mardiatno, D., Widagdo, A., Cahyadi, R., Lespinasse, N., Mahieu, L., 2006. Learning from a major disaster (Banda Aceh, December 26th, 2004): a methodology to calibrate simulation codes for tsunami inundation models. Zeitschrift für Geomorphologie. Supplementband 146, pp.253–265.

Lavigne, F., Paris, R., Grancher, D., Wassmer, P., Brunstein, D., Vautier, F., Leone F., Flohic, F., De Coster, B., Gunawan, T., Gomez, Ch., Setiawan, A., Cahyadi, R., Fachrizal, 2009. Reconstruction of tsunami inland propagation on December 26, 2004 in Banda Aceh, Indonesia, through field investigations. *Pure and Applied Geophysics*, Vol.166, pp.259-281.

Lorang, M., 2000. Predicting the threshold entrainment mass for a boulder. *Journal of Coastal Research*, Vol.16, No.2, pp.432-445.

Lorang, M., in press. A wave-competence approach to distinguish between boulder and megaclast deposits due to storm waves versus tsunamis. *Marine Geology*. doi:10.1016/j.margeo.2010.10.005.

Luccio, P.A., Voropayev, S.I., Fernando, H.S.J., Boyer, D.L., Houston, W.N., 1998. The motion of cobbles in the swash zone on an impermeable slope. *Coastal Engineering*, Vol.33, pp.41-60.

Maouche, S., Morhange, C., Meghraoui, M., 2009. Large boulder accumulation on the Algerian coast evidence tsunami events in the western Mediterranean. *Marine Geology*, Vol.262, pp.96-104.

Mastronuzzi, G., Sanso, P., 2004. Large boulder accumulations by extreme waves along the Adriatic coast of southern Apulia (Italy). *Quaternary International*, Vol.120, pp.173-184.

Mhammdi, N., Medina, F., Kelletat, D., Ahmamou, M., Aloussi, L., 2008. Large boulders along the Rabat coast (Morocco); possible emplacement by the November 1st, 1755 tsunami. *Science of Tsunami Hazards*, Vol.27, No.1, pp.17-30.

Mimura, N., Yasuhara, K., Kawagoe, S., Yokoki, H., Kazama, S., 2011. Damage from the Great East Japan Earthquake and Tsunami - A quick report. Mitig Adapt Strateg Glob Change, DOI 10.1007/s11027-011-9297-7.

Morton, R.A., Richmond, B.M., Jaffe, B.E., and Gelfenbaum, G., 2006. Reconnaissance investigation of Caribbean extreme wave deposits—Preliminary observations, interpretations, and research directions: U.S. Geological Survey Open-File Report 2006-1293 (46 p. PDF):http://pubs.usgs.gov/of/2006/1293/.

Nanayama, F., Shigeno, K., 2006. Inflow and outflow facies from the 1993 tsunami in southwest Hokkaido. *Sedimentary Geology*, Vol.187, pp.139-158.

Nandasena, N.A.K., Sasaki, Y., Tanaka, N, 2012. Modeling field observations of the 2011 Great East Japan tsunami: Efficacy of artificial and natural structures on tsunami mitigation. *Coastal Engineering*, Vol.67, pp.1-13.

Noji, M., Imamura, F., Shuto, N., 1993. Numerical simulation of movement of large rocks transported by tsunamis. Proceedings of IUGG/IOC International Tsunami Symposium, 189–197.

Noormets, R., Crook, K.A.W., Felton, E.A, 2004. Sedimentology of rocky shorelines: 3. Hydrodynamics of megaclast emplacement and transport on a shore platform, Oahu, Hawaii. *Sedimentary Geology*, Vol.172, pp.41-65.

Nott, J., 1997. Extremely high wave deposits inside the Great Barrier Reef, Australia: determining the cause-tsunami or tropical cyclone. *Marine Geology*, Vol.141, pp.193-207.

Nott, J., 2003. Waves, coastal boulders and the importance of the pre-transport setting. *Earth and Planetary Science Letters*, Vol.210, pp.269-276.

Nott, J., 2004. The tsunami hypothesis-comparison of the field evidences against the effects, on the Western Australian coast, of some of the most powerful storms on earth. *Marine Geology*, Vol.208, pp.1-12.

Paris, R., Wassmer, P., Sartohadi, J., Lavigne, F., Barthomeuf, B., Desgages, É., Grancher, D., Baumert, Ph., Vautier, F., Brunstein, D., Gomez, Ch., 2009. Tsunamis as geomorphic crisis: lessons from the December 26, 2004 tsunami in Lhok Nga, west Banda Aceh (Sumatra, Indonesia). *Geomorphology*, Vol.104, pp.59-72.

Paris, R., Fournier, J., Poizot, E., Etienne, S., Morin, J., Lavigne, F., Wassmer, P., 2010. Boulder and fine sediment transport and deposition by the 2004 tsunami in Lhok Nga (western Banda Aceh, Sumatra, Indonesia): A coupled offshore-onshore model. *Marine Geology*, Vol.268, pp.43-54.

Pignatelli, C., Sanso, P., Mastronuzzi, G., 2009. Evaluation of tsunami flooding using geomorphologic evidence. Marine Geology, Vol.260, pp.6-18.

Scheffers, A. and Kelletat, D. (2003), Sedimentologic and geomorphologic tsunami imprints world-wide – a review, *Earth-Sci. Rev.* , Vol.63, pp.83-92.

Scheffers, A., Kelletat, D., Vött, A., May, S.M., Scheffers, S., 2008. Large Holocene tsunami traces on the western and southern coastlines of the Peloponnesus (Greece). *Earth and Planetary Science Letters*, Vol.269, pp.271-279.

Scheffers, A., Kelletat, D., Scheffers, S., 2010. Wave-emplaced coarse debris and megaclasts in Ireland and Scotland: boulder transport in high-energy littoral environment: a reply. *Journal of Geology*, Vol.118, pp.705-709.

Scicchitano, G., Monaco, C., Tortorici, L., 2007. Large boulder deposits by tsunami waves along the Ionian coast of south-eastern Sicily (Italy). *Marine Geology*, Vol.238, pp.75-91.

Shiki, T., Tsuji, Y., Yamazaki, T. and Minoura, K. (2008), Tsuamiites, Features and Implications, Elsevier, The Netherlands, pp. 304-305.

Spiske, M., Borocz, Z., Bahlburg, H., 2008. The role of porosity in discriminating between tsunami and hurricane emplacement of boulders – A case study from the Lesser Antilles, southern Caribbean. *Earth and Planetary Science Letters*, Vol.268, pp.384-396.

Spiske, M., Weiss, R., Bahlburg, H., Roskosch, J., Amijaya, H., 2010. The TsuSedMod inversion model applied to the deposits of the 2004 Sumatra and 2006 Java tsunami and implications for estimating flow parameters of palaeo-tsunami. *Sedimentary Geology*, Vol.224, pp.29-37.

Switzer, A.D., Burston, J.M., 2010. Competing mechanisms for boulder deposition on the southeast Australian coast. *Geomorphology*, Vol.114, pp.42-54.

Tanaka, N., Nandasena, N.A.K., Jinadasa, K.S.B.N., Sasaki, Y., Tanimoto, K., Mowjood,

M.I.M., 2009. Developing effective vegetation bioshields for tsunami protection. *Journal of Civil and Environmental Engineering Systems*, Vol.26, pp.163-180.

Voropayev, S.I., Roney, J., Fernando, H.J.S., Boyer, D.L., Houston, W.N., 1998. The motion of large bottom particles (cobbles) in a wave-induced oscillatory flow. *Coastal Engineering*, Vol.34, pp.197-219.

Voropayev, S.I., Cense, A.W., McEachern, G.B., Boyer, D.L., Fernando, H.J.S., 2001. Dynamics of cobbles in the shoaling region of a surf zone. *Ocean Engineering*, Vol.28, pp.763-788.

Voropayev, S.I., Testik, F.Y., Fernando, H.J.S., Boyer, D.L., 2003. Morphodynamics and cobbles behavior in and near the surf zone. *Ocean Engineering*, Vol.30, pp.1741-1764.

Whelan, F., Kelletat, D. (2005), Boulder deposits on the southern Spanish Atlantic coast: possible evidence for the 1755 AD Lisbon tsunami?, *Science of Tsunami Hazards*, Vol.23, No.3, 25-38.

Williams, D.M., Hall, A.M., 2004. Cliff-top megaclast deposits of Ireland, a record of extreme waves in the North Atlantic-storms or tsunamis. *Marine Geology*, Vol.206, pp.101-117.